Supporting Information

CO_2 Electroreduction on Nano-Cu-ZIF Grown inside Activated Carbon : Experimental and Computational Aspects

Santanu Jana[a, ^], Gaurav Mukharjee[a, ^], Asmita Dutta[a], Hani Porat[a], Aneena Lal[a,b], Alon Khabra[a], Itay Pitussi[a], Arie Borenstein[a, *]

a- Department of Chemical Sciences, Ariel University, Ariel, Israel

b- Institute of chemistry, The Hebrew University of Jerusalem, Jerusalem, Israel

^- Equally contributing authors

* Corresponding author. Email: arieb@ariel.ac.il

Tables:

Table S1: Electrocatalytic performance of different MOF based and other Cu based catalysts for CO_2RR

Material	Overpotential (vs. RHE)	Current Density ($mA.cm^{-2}$)	Major product	F.E., Potential (vs. RHE)	Ref.
Ag-Cu (Ag-Cu-BTC) MOF-derived composite	−0.79 V	~-20	CO	65%, -1.8V	1
Cu-THQ / GO	−0.25 V	~-3	Formic acid	27%, -0.5V	2
CoPc-Cu-O @ carbon black	−0.63 V	~-17.3	CO	79%, -0.74V	3
Cu-HHTT	-0.60 V	~-18.0	CO	96.6%, -0.6V	4
MOF-545-Cu/PAN (MCP)	-0.8 V	~-9.0	CO	98%, -0.8V	5
Cu-Pc	-1.6 V	~-2.8	C_2H_4	25%, -1.6V	6
$Cu_3(BTC)_2$	-1.5 V	~-6.0	CH_4, C_2H_4	17% (CH_4), 16% (C_2H_4), -1.8V	7
Fe-TPP	-1.0 V	~-3.0	CO	41%, -1.3V	8
HKUST-1/C	-1.0 V	~-18.0	HCOOH	42%, -0.3V	9
Cu-Cu_2O-2	-0.4 V	~-11.5	AcOH, EtOH	48% (AcOH), 27.6% (EtOH, -0.4V	10
Cu-BTZ	-1.3V	~-7.9	AcOH	4.7%, -1.3V	11
CuO/Cu_2O	-0.9V	~-10.0	AcOH	35.78%, -0.9V	12
Cu-ZIF@AC	-0.56 V	~-10.0	AcOH	71.5%, -0.3V	This work

Table S2: Electrochemical Impedance Spectroscopy (EIS) measurement results for all the samples.

Material	**R_s (Ω)**	**R_{ct1} (Ω)**	**CPE_1 (F)**	**R_{ct2} (Ω)**	**CPE_2 (F)**
Cu-ZIF@AC	7.1 ± 0.15	4.89 ± 0.54	0.01047 ± 0.002	237.06 ± 0.28	0.1360 ± 0.005
Cu-ZIF	7.1 ± 0.38	133.98 ± 0.8	0.0004273 ± 0.0001	1053.54 ± 0.54	0.0022 ± 0.0003
AC	7.1 ± 0.17	3.91 ± 0.36	0.00255 ± 0.0006	615.65 ± 0.3	0.0886 ± 0.003

R_s = Solution resistance

R_{ct1} = Charge transfer resistance at the catalyst-electrolyte interface

CPE_1 = Capacitance at the catalyst-electrolyte interface

R_{ct2} = Diffusion limited resistance

CPE_2 = Capacitance on composite material

Table S3: Energy, Zero Point Energy (ZPE), Entropy (T*S) values for Free Systems and CO_2 adsorption from Cu_1 to Cu_{12} for Cu-MOF used in free energy calculations (T = 298.15 K).

System	Energy (eV)	ZPE (eV)	T*S (eV)
Free H_2	3.3705	0.1387	0.0560
Free CO_2	-22.9549	0.3086	0.1351
Free H_2O	-14.2185	0.5845	0.0789
Free CH_3COOH	-46.76399	1.6244	0.1615
Bulk Cu-MOF	-1756.1621	56.9270	7.8880
$Cu_1@CO_2$	-1779.3686	57.1823	8.0250
$Cu_2@CO_2$	-1779.6800	57.2484	8.0763
$Cu_3@CO_2$	-1779.7559	57.2941	8.1645
$Cu_4@CO_2$	-1779.5326	57.2734	8.1559
$Cu_5@CO_2$	-1779.5548	57.3218	8.2570
$Cu_6@CO_2$	-1779.5483	57.3016	8.1541
$Cu_7@CO_2$	-1779.3517	57.2839	8.0820
$Cu_8@CO_2$	-1779.4309	57.2883	8.1650
$Cu_9@CO_2$	-1779.4987	57.2594	8.1747
$Cu_{10}@CO_2$	-1779.4518	57.1921	8.1002
$Cu_{11}@CO_2$	-1779.5159	57.4556	7.9279
$Cu_{12}@CO_2$	-1779.5309	57.2225	7.9003

Table S4: Energy, Zero Point Energy (ZPE), Entropy (T*S) values for adsorbed species at Cu_3 site used in free energy calculations (T = 298.15 K).

System	Energy (eV)	ZPE (eV)	T*S (eV)
*OCHO	-1781.56	57.4522	8.2077
*OCHOH	-1786.87	57.7825	8.1330
*CHO	-1773.9953	57.3350	8.2536
*CHOH	-1776.8814	57.5270	8.0480
*CH_2OH	-1782.9754	58.0582	7.8423
*CH_2	-1770.6915	57.5796	7.8149
*CH_3	-1776.4685	57.8989	8.0577
*CH_3COOH	-1804.0152	58.5360	8.2255

Table S5: Energy, Zero Point Energy (ZPE), Entropy (T*S) values for adsorbed species at Cu_5 site used in free energy calculations (T = 298.15 K).

System	Energy (eV)	ZPE (eV)	T*S (eV)
*OCHO	-1781.22980222	57.5540	7.9795
*OCHOH	-1786.28595098	57.8073	8.0869
*CHO	-1773.44423226	57.2061	8.0743
*CH_2O	-1778.78037319	57.6238	8.1258
*CH_2OH	-1781.54046811	57.8840	8.0667
*CH_2	-1768.42238507	57.4627	7.9226
*CH_3	-1774.57171817	57.8548	7.9724
*CH_3COOH	-1803.42757475	58.4199	8.1957

Table S6: Energy, Zero Point Energy (ZPE), Entropy (T*S) values for adsorbed species at Cu_7 site used in free energy calculations (T = 298.15 K).

System	Energy (eV)	ZPE (eV)	T*S (eV)
*COOH	-1782.7793	57.4990	7.9174
*CO	-1771.5168	57.0601	8.0265
*CHO	-1773.5940	57.2270	8.0029
*CH_2O	-1778.9464	59.6941	8.1383
*CH_2OH	-1782.2131	57.8535	7.9568
*CH_2	-1768.7533	57.3626	7.9711
*CH_3	-1774.9373	57.6676	7.9424
*CH_3COOH	-1803.6931	58.5710	8.1329

Figures:

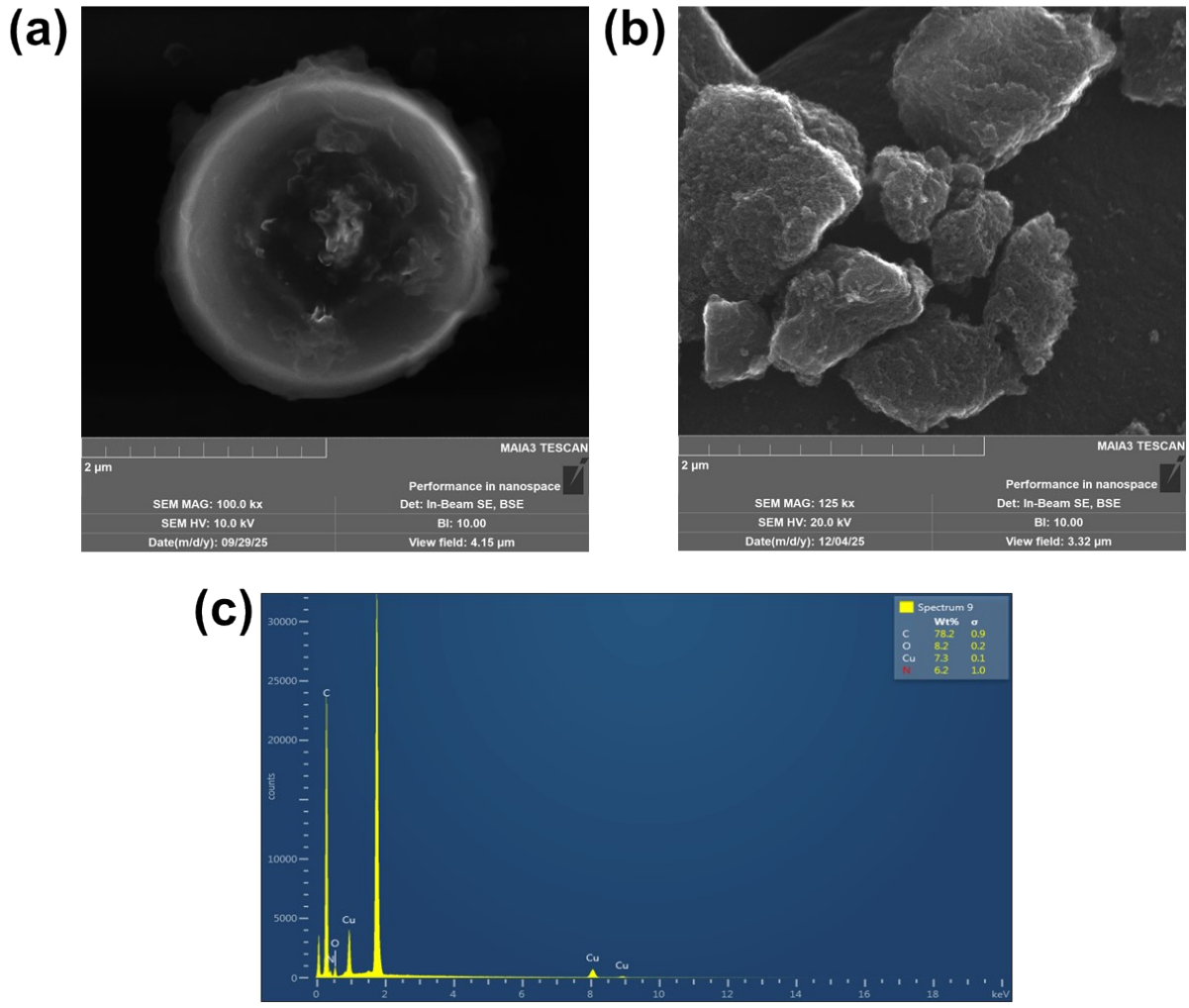

Figure S1: SEM images of pristine Cu-ZIF (a) and the Cu-ZIF@AC (b) are shown. In the composite, typical activated carbon particles are seen, with only minor MOF deposition observed on the surface, indicating that the MOF is predominantly confined within the carbon pores rather than on the external surface. The SEM-EDX elemental analysis is shown in (c).

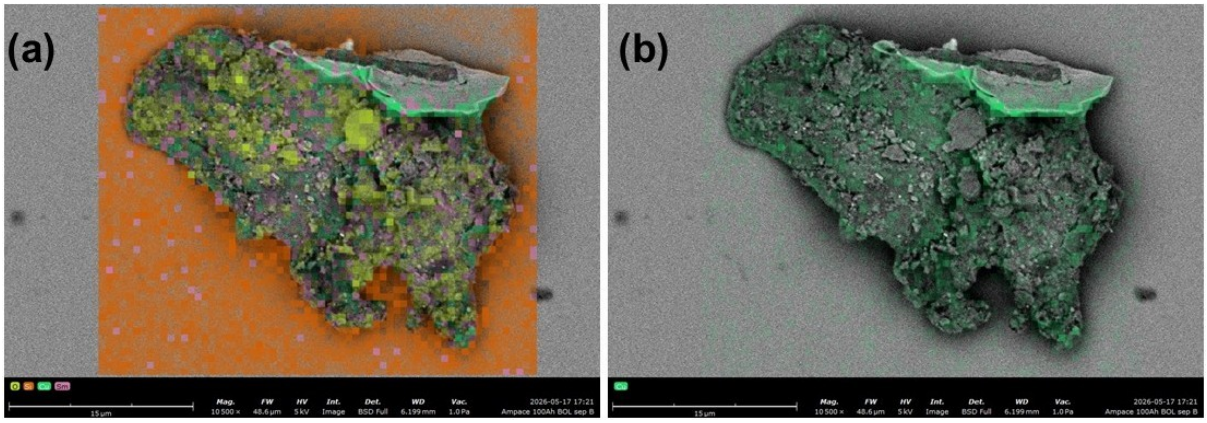

Figure S2: SEM-EDX Mapping images of Cu-ZIF@AC. The Cu elemental signal is uniformly distributed throughout the entire Activated Carbon without the presence of localized Cu-rich regions.

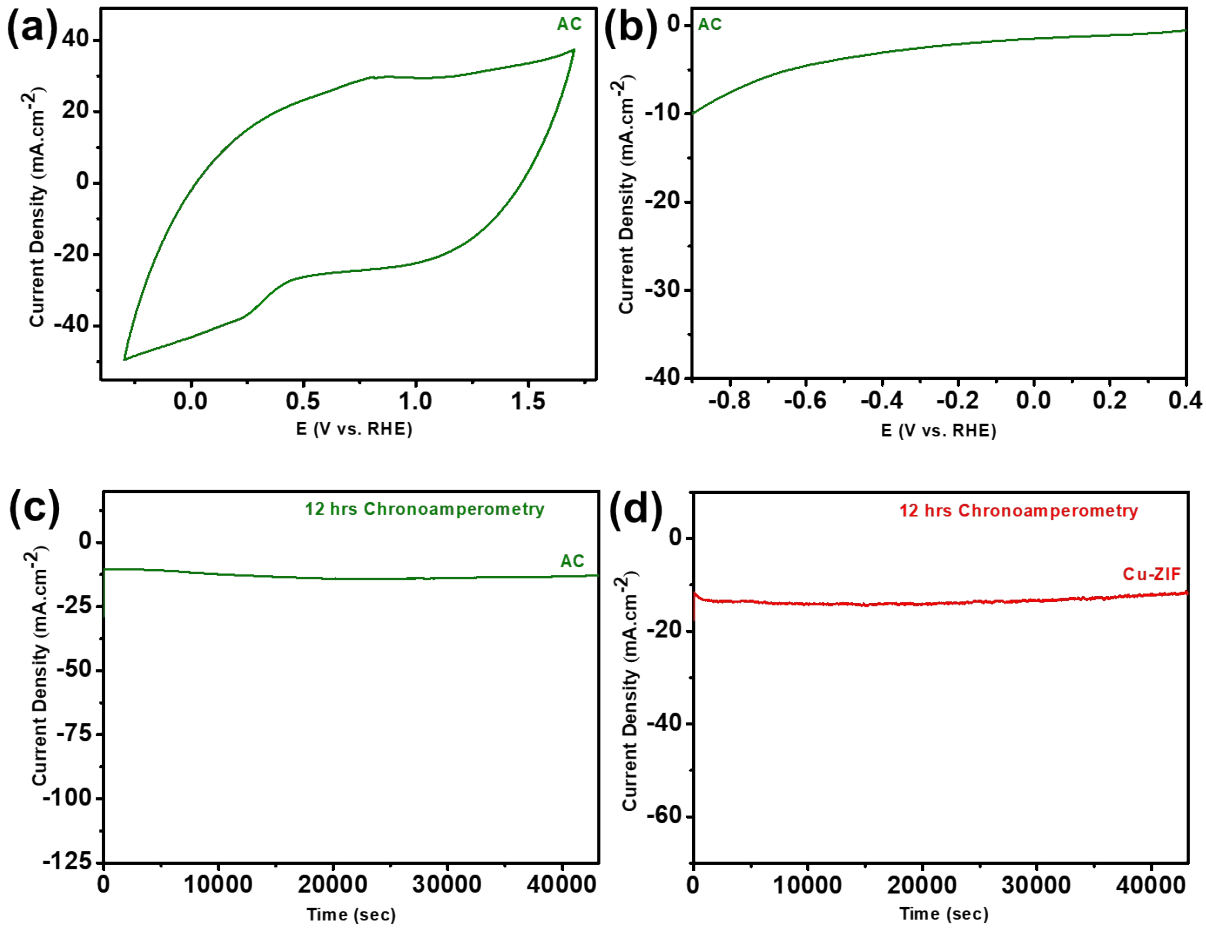

Figure S3: (a) Cyclic Voltammetry (CV) curve of activated carbon coated on 1cm^2 of carbon paper in N_2 purged 0.5M Na_2SO_4; (b) Linear Sweep Voltammetry (LSV) of Activated carbon in CO_2 purged 0.5M $KHCO_3$; (c)12 hrs of stability test using Chronoamperometry for AC in CO_2 saturated 0.5 M $KHCO_3$ at constant potential of -0.9 V vs. RHE; (d) 12 hrs of stability test using Chronoamperometry for Cu-ZIF in CO_2 saturated 0.5 M $KHCO_3$ at constant potential of -0.72 V vs. RHE.

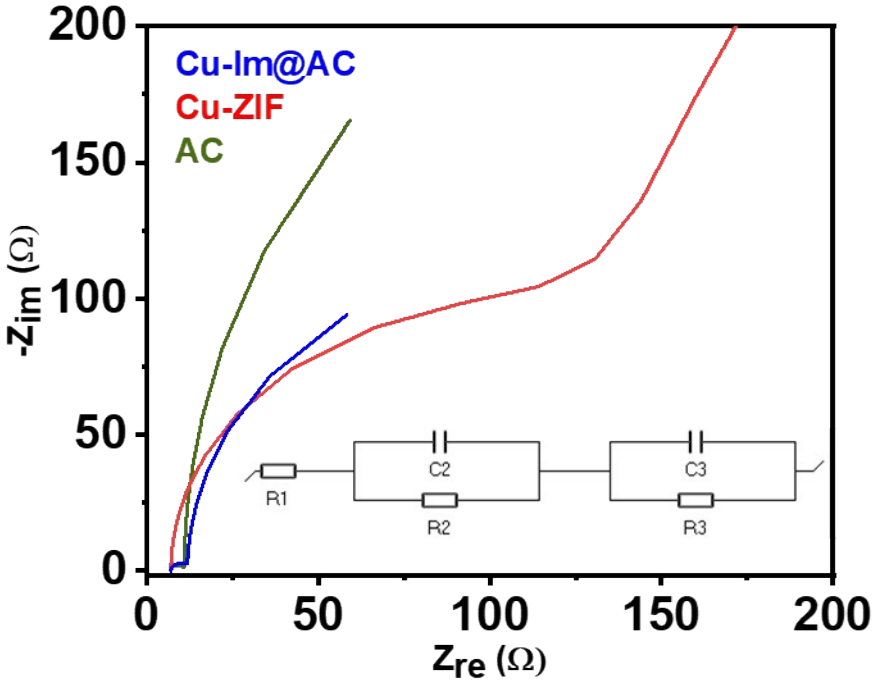

Figure S4: Nyquist plots of Cu-ZIF@AC, Cu-ZIF, AC along with the fitted curves obtained from Electrochemical Impedance Spectroscopy (EIS) measured in CO_2 purged 0.5M $KHCO_3$ using the equivalent circuit model shown inset, where R_1 = Solution resistance; R_2= Charge transfer resistance at the catalyst-electrolyte interface; C_2 = Capacitance at the catalyst-electrolyte interface; R_3 = Diffusion limited resistance; C_3 = Capacitance on composite material.

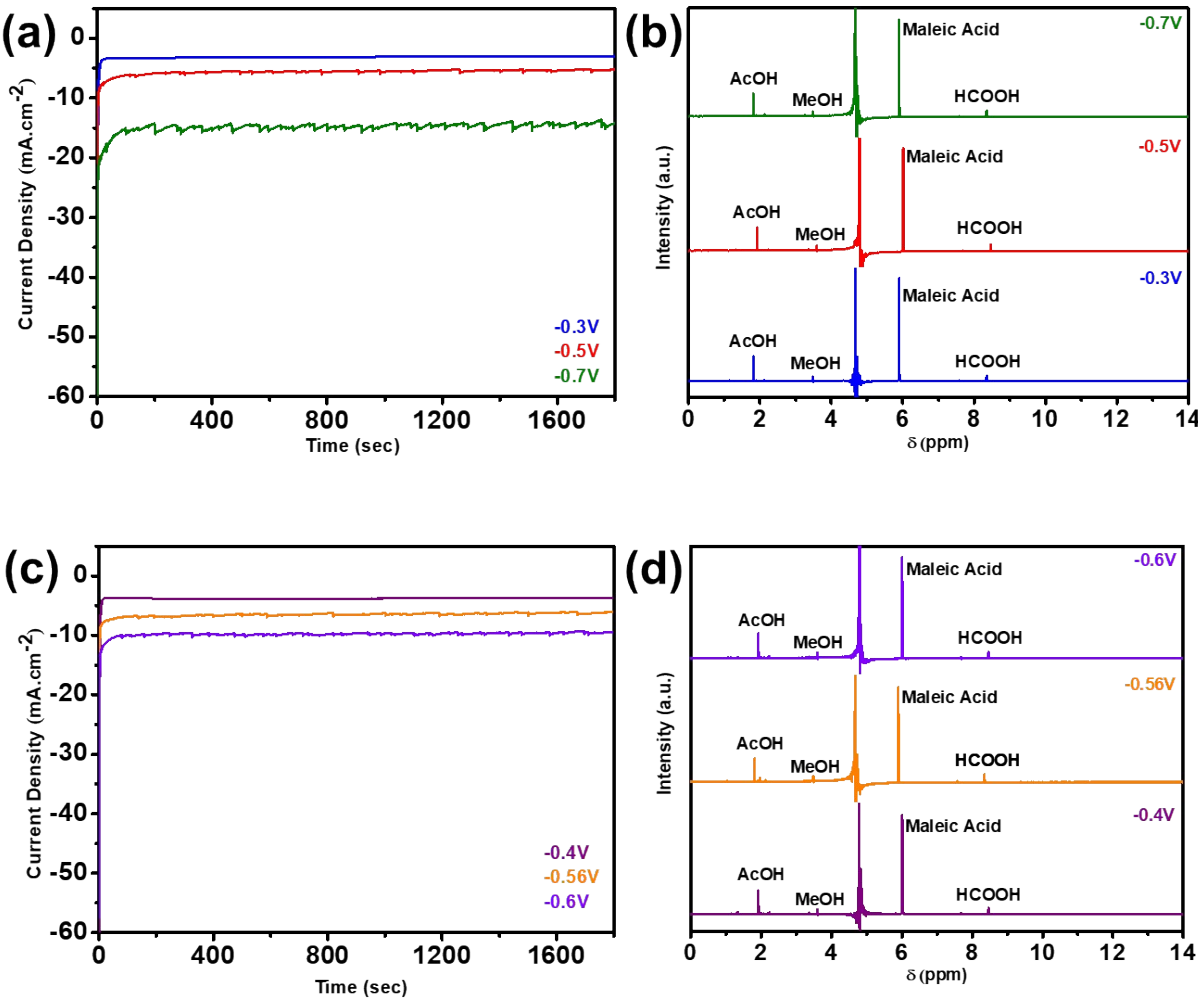

Figure S5: Chronoamperometry plots (a), (c) of Cu-ZIF@AC coated on carbon paper electrode at different potentials (vs. RHE) in CO_2 purged 0.5M $KHCO_3$ electrolyte are shown. The NMR spectra (b), (d) of the products were analysed using 400 MHz NMR after collection of electrolytes at 30 minutes of Chronoamperometry where Maleic acid was used as internal standard.

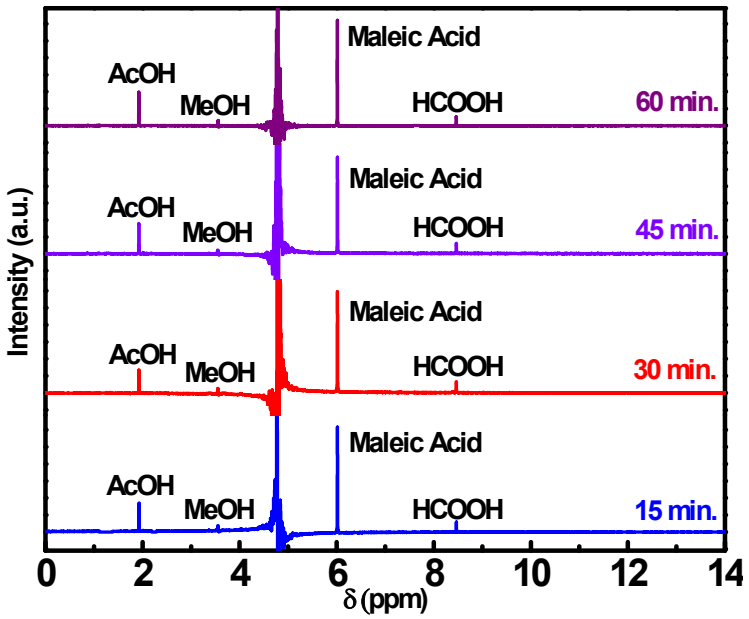

Figure S6: The NMR spectra of the products were analysed using 400 MHz NMR after collection of electrolytes at 15-60 minutes of Chronoamperometry at -0.3 V vs. RHE where Maleic acid was used as internal standard.

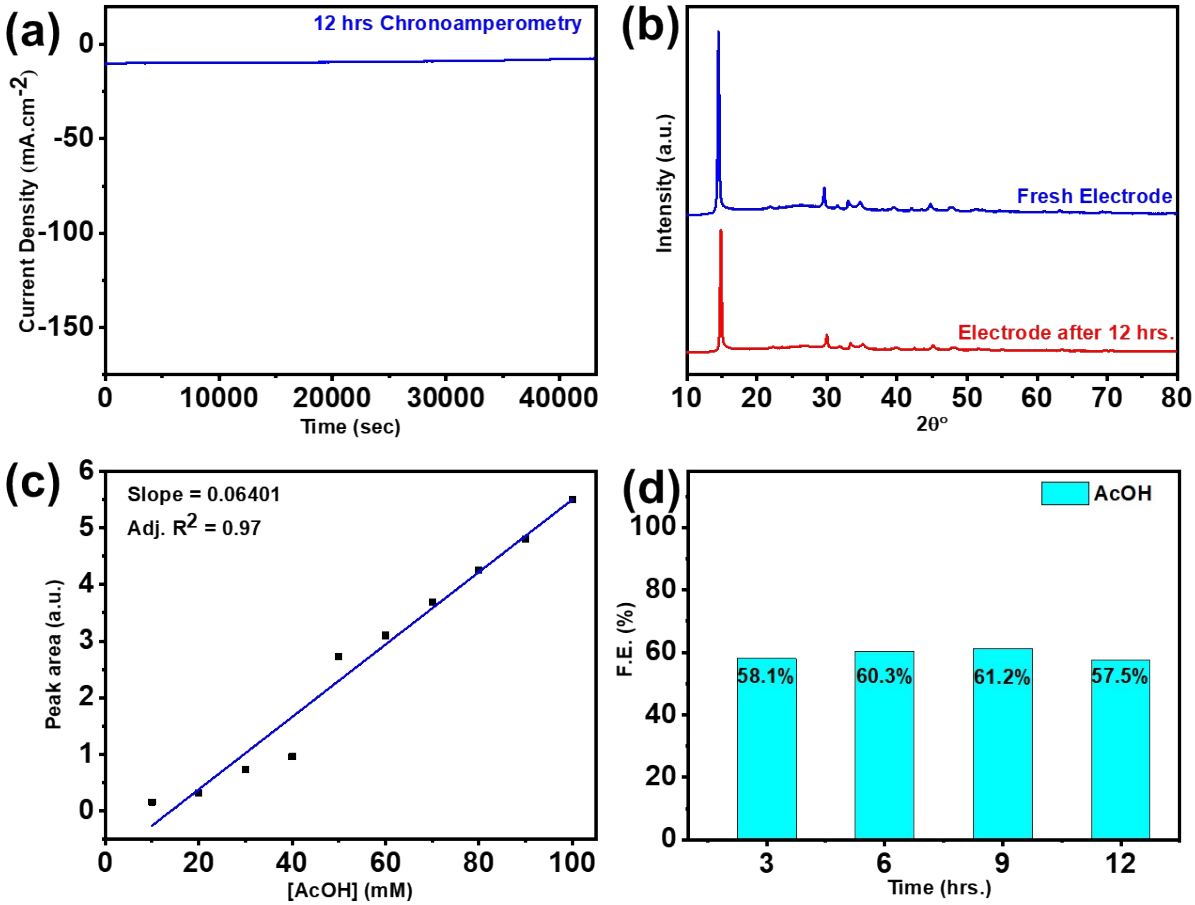

Figure S7: (a) 12 hrs of stability test using Chronoamperometry for Cu-ZIF@AC in CO_2 saturated 0.5 M $KHCO_3$ at constant potential of -0.56 V vs. RHE exhibiting stable 10 mA.cm^{-2}current density; (b) PXRD data of Cu-ZIF@AC before and after 12 hrs. of Chronoamperometry; (c) Calibration curve for AcOH using Gas Chromatography; (d) Faradaic Efficiency (F.E.) at different time intervals during the 12 h chronoamperometry.

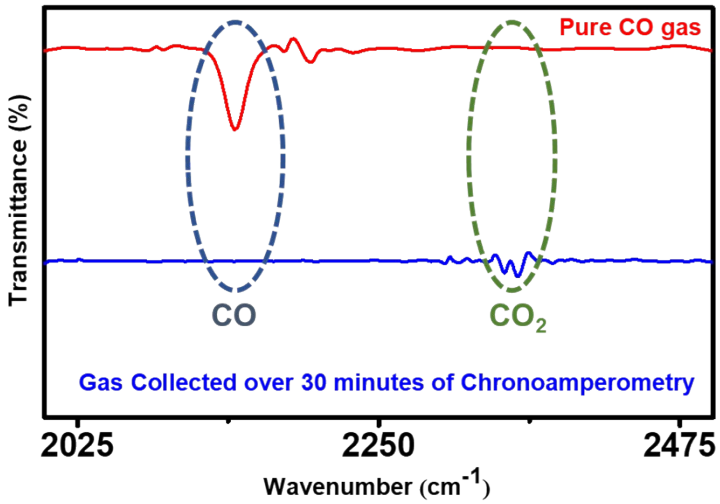

Figure S8: The Gas FTIR Spectra of Pure CO and gas collected over 30 minutes of Chronoamperometry of Cu-ZIF@AC at -0.3V vs. RHE in CO_2 purged 0.5M $KHCO_3$ solution. The corresponding CO and CO_2 peaks are shown here. The CO_2 peak arises due to purging of CO_2 in 0.5M $KHCO_3$ solution before Chronoamperometry.

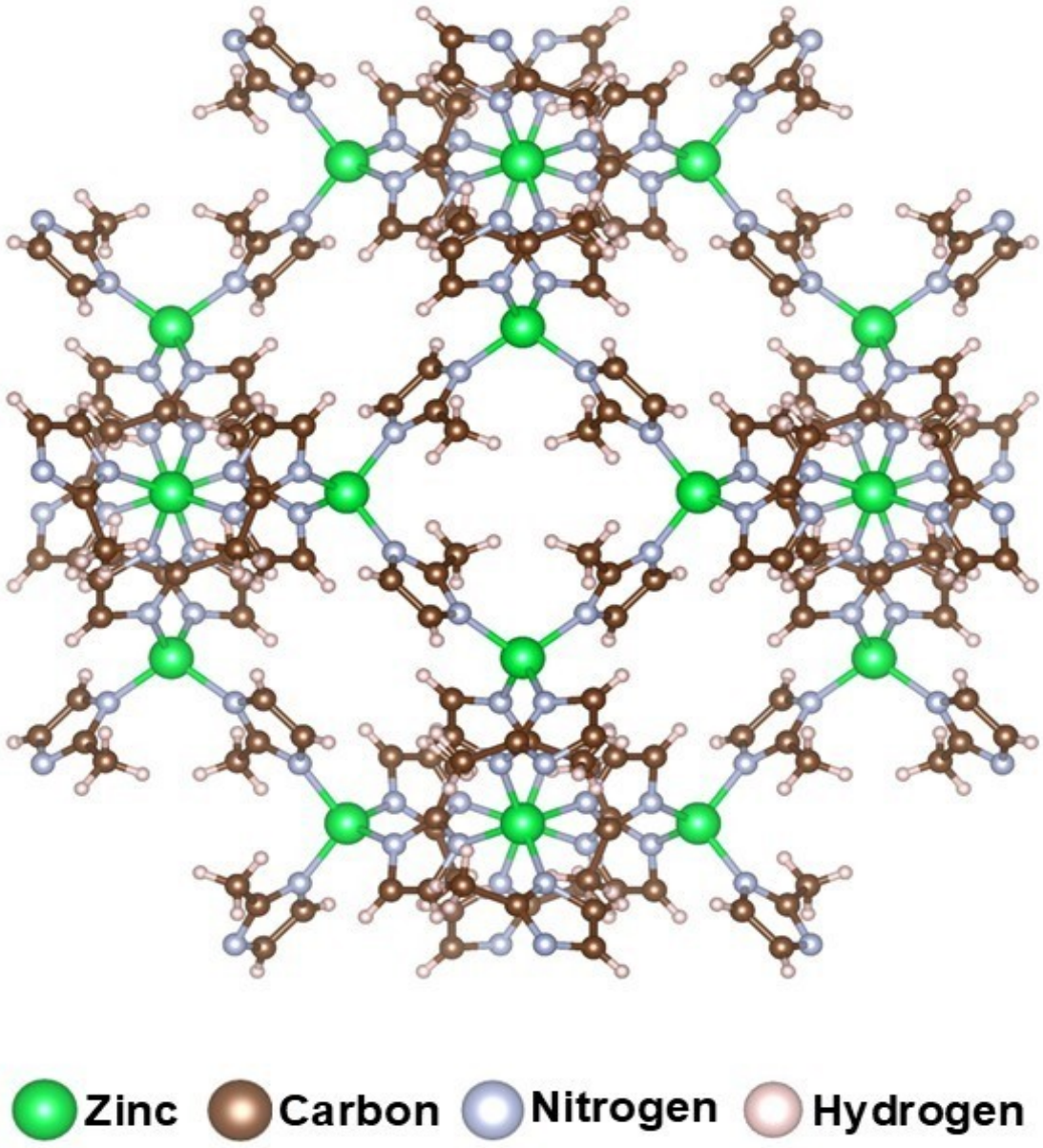

Figure S9: - Structure of ZIF-8.

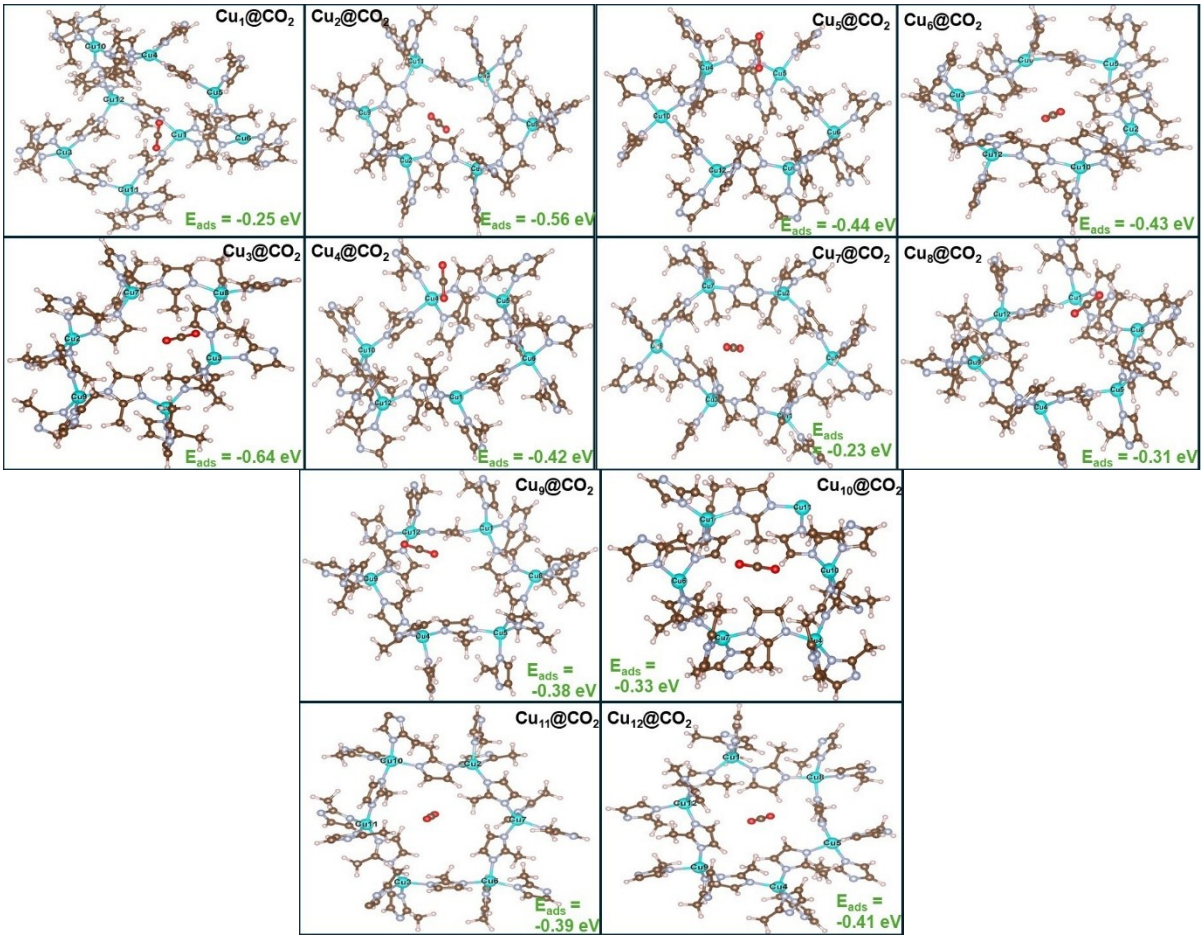

Figure S10: - The adsorption reaction energies for CO_2 adsorption on Cu_1 to Cu_{12} for Cu-ZIF.

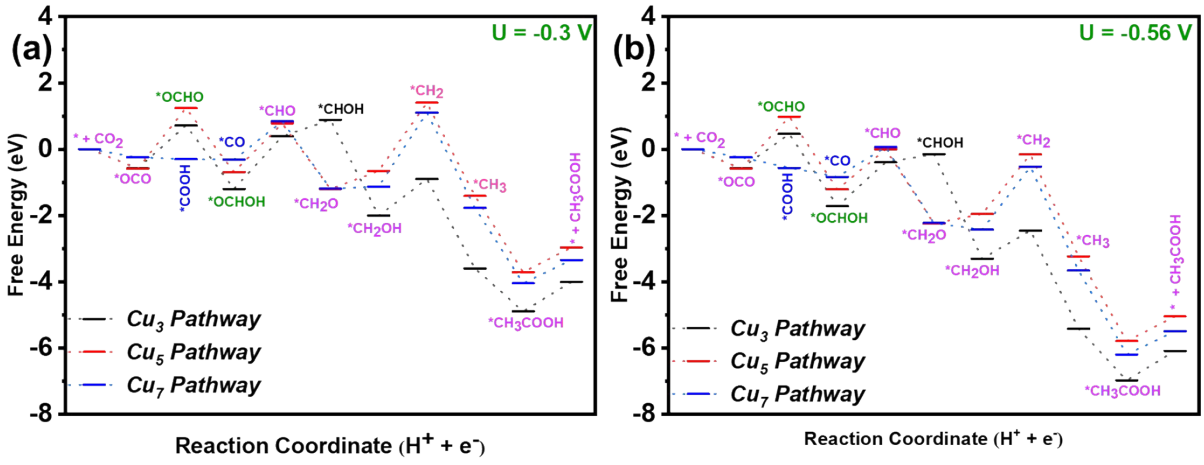

Figure S11: Free energy profile for CO_2 to CH_3COOH on Cu-ZIF at Cu_3, Cu_5, Cu_7 sites (a) -0.3 V and (b) - 0.56 V. Black, Red, Blue legends represent the CH_3COOH pathway for Cu_3, Cu_7, Cu_5 copper adsorbing sites in the Cu-ZIF, respectively.

References

(1) Nambi, A.; Chatzitakis, A.; Olsbye, U.; Hjelm, J.; Zhao, Y.; Kaiser, A. Gas-Phase Electrochemical CO2 Reduction on Silver-Copper BTC MOF in a Zero-Gap Membrane Electrode Assembly. *Electrochim. Acta* **2024**, *506*, 144763.

(2) Jia, L.; Wagner, K.; Smyth, J.; Officer, D.; Chen, J.; Wagner, P. Cu-THQ-EFG Composite for Highly Selective Electrochemical CO2 Reduction to Formate at Low Overpotentials. *Polymers (Basel).* **2022**, *14* (23), 5112.

(3) Meng, Z.; Luo, J.; Li, W.; Mirica, K. A. Hierarchical Tuning of the Performance of Electrochemical Carbon Dioxide Reduction Using Conductive Two-Dimensional Metallophthalocyanine Based Metal–Organic Frameworks. *J. Am. Chem. Soc.* **2020**, *142* (52), 21656–21669.

(4) Xue, H.; Zhu, H.; Huang, J.; Liao, P.; Chen, X. Ultrathin Two-Dimensional Triptycence-Based Metal-Organic Framework for Highly Selective CO2 Electroreduction to CO. *Chinese Chemical Letters* **2023**, *34* (1), 107134.

(5) Xin, Z.; Yuan, Z.; Liu, J.; Wang, X.; Shen, K.; Chen, Y.; Lan, Y.-Q. Cu Cluster Embedded Porous Nanofibers for High-Performance CO2 Electroreduction. *Chinese Chemical Letters* **2023**, *34* (4), 107458.

(6) Kusama, S.; Saito, T.; Hashiba, H.; Sakai, A.; Yotsuhashi, S. Crystalline Copper(II) Phthalocyanine Catalysts for Electrochemical Reduction of Carbon Dioxide in Aqueous Media. *ACS Catal.* **2017**, *7* (12), 8382–8385.

(7) Qiu, Y.-L.; Zhong, H.-X.; Zhang, T.-T.; Xu, W.-B.; Su, P.-P.; Li, X.-F.; Zhang, H.-M. Selective Electrochemical Reduction of Carbon Dioxide Using Cu Based Metal Organic Framework for CO_2 Capture. *ACS Appl. Mater. Interfaces* **2018**, *10* (3), 2480–2489.

(8) Hod, I.; Sampson, M. D.; Deria, P.; Kubiak, C. P.; Farha, O. K.; Hupp, J. T. Fe-Porphyrin-Based Metal–Organic Framework Films as High-Surface Concentration, Heterogeneous Catalysts for Electrochemical Reduction of CO_2. *ACS Catal.* **2015**, *5* (11), 6302–6309.

(9) Sathiyan, K.; Dutta, A.; Marks, V.; Fleker, O.; Zidki, T.; Webster, R. D.; Borenstein, A. Nano-Encapsulation: Overcoming Conductivity Limitations by Growing MOF Nanoparticles in Meso-Porous Carbon Enables High Electrocatalytic Performance. *NPG Asia Mater.* **2023**, *15* (1), 18.

(10) Zhu, Q.; Sun, X.; Yang, D.; Ma, J.; Kang, X.; Zheng, L.; Zhang, J.; Wu, Z.; Han, B. Carbon Dioxide Electroreduction to C2 Products over Copper-Cuprous Oxide Derived from Electrosynthesized Copper Complex. *Nat. Commun.* **2019**, *10* (1), 3851.

(11) Zhu, H.-L.; Chen, H.-Y.; Han, Y.-X.; Zhao, Z.-H.; Liao, P.-Q.; Chen, X.-M. A Porous π–π Stacking Framework with Dicopper(I) Sites and Adjacent Proton

Relays for Electroreduction of CO_2 to C_{2+} Products. *J. Am. Chem. Soc.* **2022**, *144* (29), 13319–13326.

(12) Zhang, K.; Chen, S.; Ge, Y.; Zhang, X.; Zhang, Z.; Ye, C.; Pan, G.; Hu, L. CuO/Cu_2O Catalyst with Adjustable Cu(II)/Cu(I) for Selective CO_2 Electroreduction to Acetate. *ACS Appl. Nano Mater.* **2025**, *8* (46), 22285–22294.